This is a peer-reviewed, accepted author manuscript of the following article: Galdámez-Martínez, A., Bai, Y., Santana, G., Sprick, R. S., & Dutt, A. (2020). Photocatalytic hydrogen production performance of 1-D ZnO nanostructures: role of structural properties. *International Journal of Hydrogen Energy*. https://doi.org/10.1016/j.ijhydene.2020.08.247

Photocatalytic hydrogen production performance of 1-D ZnO nanostructures: Role of Structural Properties

A. Galdámez-Martínez[a], Yang Bai[b], G. Santana[a, *], Reiner Sebastian Sprick[b,c *], and A. Dutt[a,*]

[a] *Materials Research Institute, National Autonomous University of Mexico, Coyoacan, México City 04510, Mexico*
[b] *Materials Innovation Factory and Department of Chemistry, University of Liverpool, Crown Street, Liverpool L69 7ZD, UK*
[c] *Department of Pure and Applied Chemistry, University of Strathclyde, Thomas Graham Building, 295 Cathedral Street, Glasgow G1 1XL, UK*

[*]Corresponding author.
E-mail address: sebastian.sprick@strath.ac.uk (R. S. Sprick), gsantana@iim.unam.mx (G. Santana) and adutt@iim.unam.mx (A. Dutt)

ABSTRACT

We report the synthesis of zinc oxide (ZnO) nanowires (NWs) grown via vapor-liquid-solid (VLS) process using Gold (Au) as a catalyst metal on aluminum-doped zinc oxide (AZO) seed layer. During the growth procedure, the nucleation process helps us to obtain ZnO nanowires with Au on the tip, confirming the VLS growth mechanism. Different morphologies were obtained after the variation in the growth parameters in the VLS technique, and further, their role in the photocatalytic performance was studied. Changes in the structural properties of nanowires allowed us to modify the aspect ratio and surface area of the nanostructures. X-ray diffraction (XRD) showed that the principal orientation of the nanowires was (002) in the present case. Scanning electron microscopy (SEM) showed the structural properties of 1-D nanostructures (nanowires), and statistical analysis revealed that the average diameter in the present case was found to be varied from 57 to 85 nm. Scanning transmission electron microscopy (STEM)

technique revealed the different elements present on the surface of ZnO NWs. Further, the compositional profile of nanostructures was cross-verified using Energy-dispersive Spectroscopy (EDS). Photoluminescence (PL) and UV Visible studies were employed to study the optical properties of nanowires. UV-Vis measurements showed the role of different structural properties of nanowires on the absorption spectra, especially in the visible region. The ZnO nanowires were tested as photocatalysts for hydrogen production from water splitting reaction, and it was found in particular nanowires with random orientation with optimal diameter distribution show the stable and highest photocatalytic performance.

Keywords: ZnO Nanowires, Morphological and optical properties, Photocatalysis, Hydrogen production

1. Introduction

The worldwide energy demand continues to rise to unprecedented levels due to the increase of the global population and increased development in many countries compared to the last decades [1]. Today, most of this energy is generated by the burning of different kinds of fossil fuels (i.e., oil, gas, or coal), which results in the production of CO_2 and which is further affecting the climate on Earth, as a known greenhouse gas. Combined with the fact that fossil fuels have limited availability and a drop in production in the coming decades is expected, it has led to the study of hydrogen as an energy vector that is carbon-neutral and its combustion in fuel cells only produces water.

Hydrogen is one of the ideal clean fuel of the future because of its high energy density compared to other conventional fuels. It is also one of the most abundant elements existing in both water and biomass [2]. However, the production of hydrogen and storing continue the main issues in moving towards a hydrogen economy due to the complexity of the processes and high energetic costs. Up-to-date marketable hydrogen

manufacture relies on steam-reforming obtained from non-renewable resources [3], which could also result in the emission of large amounts of carbon dioxide [4].

Since the discovery of photocatalytic hydrogen production by Honda and Fujishima in 1972 [5], it is considered as a promising energy source in the future[6]. Over the last few decades, extensive research on different materials for photocatalytic hydrogen production has been made, either by direct water splitting process or by the decomposition of organic compounds and biomass [7-12].

Many photocatalytically active materials for hydrogen production from water have been studied [8], for example, metal oxides [3], sulfides [9], nitrides [10], oxysulfides [11], carbon nitrides [12] and oxynitrides [13]. TiO_2 [7] and ZnO [14] are among the most extensively studied materials. Furthermore, ZnO exhibits a wide direct bandgap of 3.30-3.37 eV at 300K, as well as the binding energy of 60 meV for free excitons [14-15]. These two characteristics make the ZnO as an attractive candidate in a wide range of optical and electronic applications [16]. Since the electron mobility of ZnO is higher than that of TiO_2 [17], the efficiency in the electronic transfer is increased, and the losses by recombination processes are also reduced.

ZnO possesses a suitable band structure meeting the thermodynamic requisites for water splitting. It is also a low cost, non-toxic material, and possesses a high degree of crystallinity, and stability as a photocatalyst. Even when the conversion efficiency of ZnO is lower compared to some metal sulfide semiconductor systems [6], its facility of crystallization and anisotropic growth make it an attractive alternative over other photocatalysts such as ZnS, CuS or other core-shell structures [18].

However, the ZnO structures have an intrinsic limitation. They are more active under ultraviolet light [19], which only accounts for $\sim$3 % of the sunlight that reaches the Earth's surface. Therefore, considerable effort has been made to increase the

photoresponse of the material in the visible region using different strategies [3,18-19].

Currently, the advantages of using 1-D structures (e.g., nanorods (NRs), nanowires (NWs), nanotubes(NTs), nanobelts (NBs)) over the exciton separation efficiency has been studied due to the specific built-in potential gradients of these kinds of nanostructures [21]. Another essential feature of the NWs is their fast electron movement along the central axis of the wire. Successively, this improvement will result in the collection time of electrons. Contrarily, an electron scattering effect is generally observed in the grain boundaries of polycrystalline films, which drastically reduce the performance of the device. For this reason, single crystalline or defect-free nanowire structures are desired, as they present few-electron traps sites [22].

Nevertheless, another of the main limitations regarding the usage of ZnO as photocatalysts is the effective separation of photogenerated charge carriers. Different approaches are being investigated, and it has been found that one of the possibilities could be the introduction of the Fermi level of a noble metal, usually of lesser energy than the semiconductor conduction band. With this approach, electrons can move upwards towards the noble metal, whereas holes can stay in the valence band [8]. This mechanism can work synergistically with a surface plasmon resonance effect to produce what is known as “plasmonic photocatalysis” [23–25]. For that reason, the practical implementation of Au and Ag NPs in materials such as TiO_2[26] and MoS_2 [27] (hydrothermal synthesized systems) have reported an enhancement of the hydrogen evolution ratio (HER).

Different methods have been explored for the growth of these 1-D nanostructures. In general, bottom-up techniques are preferred due to the control they offer over the morphology, orientation, and composition of the obtained nanostructures [28].

In general, chemical synthesis techniques such as hydrothermal [29], solvothermal

[30], or different variants of the CVD technique[31] are the most reported for obtaining nanowire structures as they can be carried out at low temperatures over organic substrates. However, to achieve a good crystalline structure as well as precise alignment between the nanowires and the substrate, high-temperature physical techniques are required. Among them, the vapor-liquid-solid (VLS) technique is one of the most versatile in the growth of NW arrays in a reproducible manner [32,33]. The flexible nature of this technique also offers the advantage to vary different deposition conditions, which could subsequently result in the various structural properties.

The technique is categorized as a metal-assisted vapor phase transport technique in which gas precursors of the nanowire structure dissolve into a liquid catalytic metal nanoparticle previously deposited over the substrate. Then, when supersaturation conditions are reached, a crystal structure nucleates below the catalyst leading to the growth of the nanowire. After that, the growth depends on factors such as the presence of source materials or the process temperature.

After having experience in the use of VLS technique for the obtention of various ZnO nanowires morphologies [28], hereby, the current manuscript sheds light on the conditions (temperature of the substrate, the crystalline orientation of the seed layer, and the use of different mixtures of carrier gases) to obtain crystalline, morphological controlled, and pure 1D ZnO nanostructures. Variation in the growth parameters in the VLS technique allowed us to tune the aspect ratio, surface area, and morphology of the nanowires to find an appropriate structure with maximum absorption. Suitable diameter with optimal properties was found for the stable and best photocatalytic performance on the water-splitting reaction. To the extent of our knowledge, there are almost no articles where the hydrogen evolution from ZnO nanowires grown by VLS technique with variable structural properties has been presented.

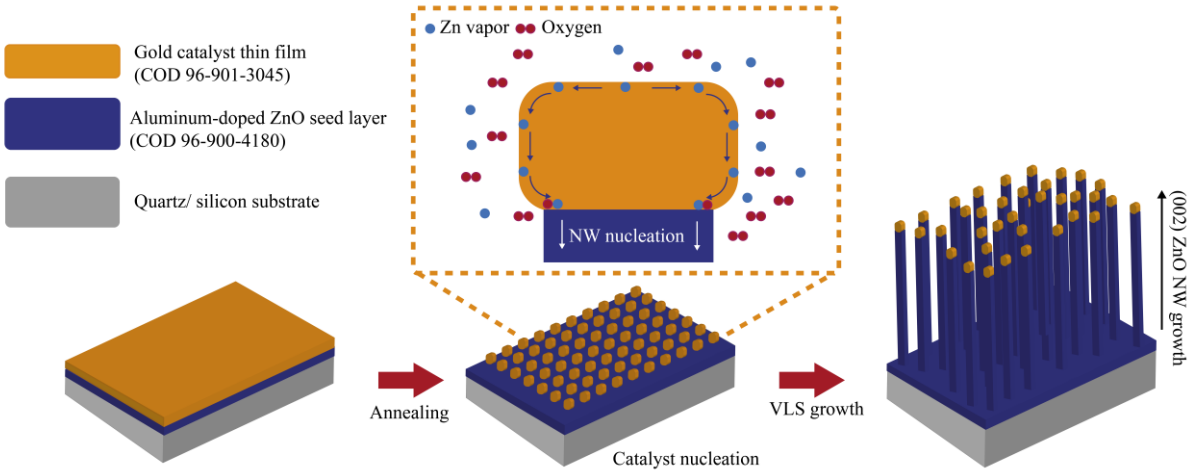

2. Experimental

2.1. Nanowires growth process

Scheme 1. Graphical representation of the experimental procedure followed for the obtention of ZnO nanowires. The main stages of the Vapor-Liquid-Solid growing mechanism (i.e., metal catalyst nucleation, diffusion of the vapor species, anisotropic nanowire crystal growth) are presented.

In general, ZnO nanowires growth via VLS process is shown in Schematic 1. As can be seen, Silicon (100) and quartz substrates (1” × 1”) were used for the growth process. For the stepwise growth mechanism and other essential details, please refer to our previous published work [25].

2.2 Characterization techniques

Different techniques were employed to study the different properties of nanowires. RIGAKU Ultima IV apparatus was used to study the orientation properties of nanowires. ZnO zincite (969004180) and gold (969013045) database sheets from the open crystallographic database (COD) were used to identify the crystallographic phases

of the samples.

JEOL JSM-7600F equipped with different detectors was used to study the morphological properties of the nanowires. Further, for the TEM study (orientation, crystalline property, and compositional mapping), JEOL JEM-201 equipped with LaB6 filament and STEM detector was used. Energy dispersive spectroscopy (EDS) measurements were also performed to confirm and cross-check the STEM analysis. X-ray photoelectron spectra measurements were performed with a PHI 5000 VersaProbe II XPS microscope to obtain information about the chemical state and electronic structure of the samples.

For the study of the optical properties, a Kimmon Koha He-Cd laser (325 nm) was used to measure the Photoluminescence (PL) spectra of the samples. In addition, a Filmetrics F10-RT-UV spectrometer equipped with both a deuterium and halogen lamp was used for the reflectance measurement.

2.3 Photocatalysis experiments

The photocatalytic film sample was placed in water in the presence of a mixture of Na_2S and Na_2SO_3 as a sacrificial electron donor. The reactor was degassed by nitrogen bubbling for 30 minutes. 300 W Newport Xenon light-source (Model: 6258, Ozone free) was used for the time-course kinetic experiments, and it was cooled by water circulating through a metal jacket. All experiments were carried out under atmospheric pressure. The gas analysis was determined by a gas chromatograph (Bruker 450-GC) fortified with an Ar flow, and a thermal conductivity detector was used in GC for H_2 detection. A standard gas sample with fixed concentration hydrogen was used for GC calibration. H_2 in water can not be measured, and increased pressure by photocatalytic gas evolution was neglected in the calculations. A mixture of water/Na_2S/Na_2SO_3 without

photocatalyst can not produce any H_2 under $\lambda > 295$ nm illumination from a blank control experiment [34].

3. Results and discussion

3.1. Structural properties

Fig. 1 illustrates the X-ray diffraction patterns for the ZnO NWs grown by the VLS technique. In these patterns, all the samples showed polycrystalline features. Regardless of the NW growth, samples C1, C2, C3, and C4 maintained the same dominant peak at approximately 34.33° corresponding to (002) plane. For the sample C5, in which the substrate temperature was significantly lower than in the other samples, the pattern showed different crystallographic orientations like (100), (101), (102), and (110) with the primary orientation towards (103) peak. The difference appearing in the main diffraction peak clearly remarks the transition of the growth regime of the nanostructure, from VLS to VS. For the first four samples, (002) peak observed can be correlated with the c-orientation. This, along with the epitaxial growth of the structure, determines the spatial orientation of the nanowires. Moreover, a gold peak (COD 96-901-3045 database sheet) corresponding to the metal catalyst employed is also presented in all the patterns. Also, the grain size (Gs) calculation of the nanocrystals in the nanowires calculations was performed using Scherer's equation [35].

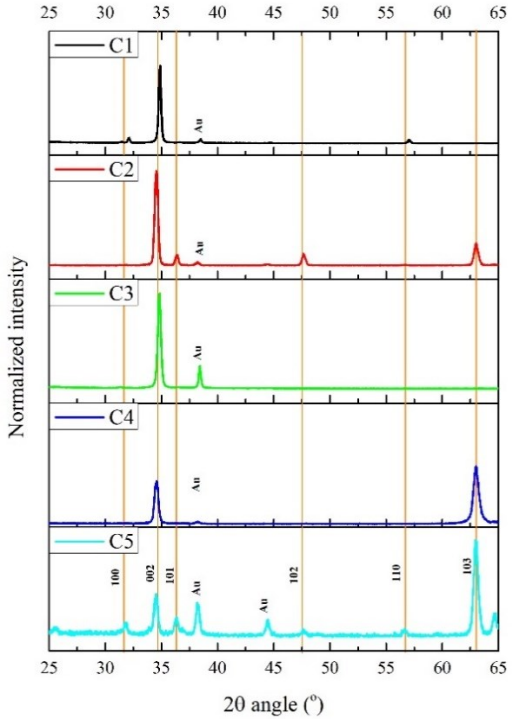

Fig. 1. XRD patterns of ZnO nanowires samples (C1 to C5). Measurements were made at a grazing angle of 2 degrees.

Even though the growth conditions for samples C1 to C4 are quite the same, significant difference can be found in the seed layer orientations (C2) and the Ar/O2 ratio (C3 and C4). Figure S1 of the Supporting Information shows the XRD patterns of the AZO seed layers used for the VLS growth of the ZnO nanowires samples. As shown in this figure, samples that were later found to have grown with high vertical alignment (C1 and C3) correspond to the ones where exclusively (002) orientated seed layer films were used, so that a preferential growth in this direction was achieved. On the other hand, for the C2 sample where (103) peak was also presented; multiple orientated ZnO nanowires were obtained. These results corroborate the epitaxial relation between the grown nanostructure and the employed seed layer.

On the other hand, for samples C3 and C4 the effect of the lower O_2 concentration in the carrier gas mixture was evaluated as significantly shorter structures were found to grow over the two types of AZO seed layers. With these results, two growth-driving

forces of the VLS technique, epitaxial and chemical parameters are explored. The morphological and structural parameters are presented in Table 1.

Table 1. Growth conditions and structural parameters of the samples of ZnO nanowires synthesized by VLS technique. A mixture of ZnO powder and graphite was used for carbothermal reduction in 1:1 ratio using an Ar flow of 8.33×10^{-6} m^3/s for 60 min. Grain size (Gs) calculations were performed using Scherer's equation [35]. Diameter, length, and aspect ratio (ratio of length/diameter) were obtained by electron micrograph analysis.

		Morphological parameters			
Sample	Temperature [°C]	Gs	D [nm]	L [mm]	Aspect Ratio
C1	950	27.4±3.4	57±16	2.77±0.51	49±23
C2	950	22.9±1.4	85±24	2.55±0.55	43±19
C3	950	23.2±1.1	56±12	2.19±0.39	39±15
C4	950	19.5±1.7	62±18	0.77±.25	12±8
C5	400	15.1±1.8	-	-	-

3.2. Morphological properties

Fig. 2 illustrates SEM micrographs of the ZnO nanowires grown by VLS technique, where a change in the morphology as a function of growth condition can be observed. SEM images show that the obtained nanowires grow mainly in two angles (directions). Many nanowires grow vertically (002 crystallographic orientation), forming an angle of almost 90° to the substrate (Si, SiO_2) plane in the case of samples C1 and C3. In these two samples, we obtain highly vertically orientated nanowires with good homogeneity throughout the substrate. We observe that the nanowires, in some cases, also grow at a tilted angle around 65° (C2 sample). We can attribute the growth in this direction to the presence of a second family of crystallographic planes present on the superficial area of the thin film of AZO used as a seed layer. SEM images show features that match with the results that are expected based on the XRD spectra, i.e., patterns

that are dominated by a single diffraction peak corresponding to the high-orientated structure in the micrographs.

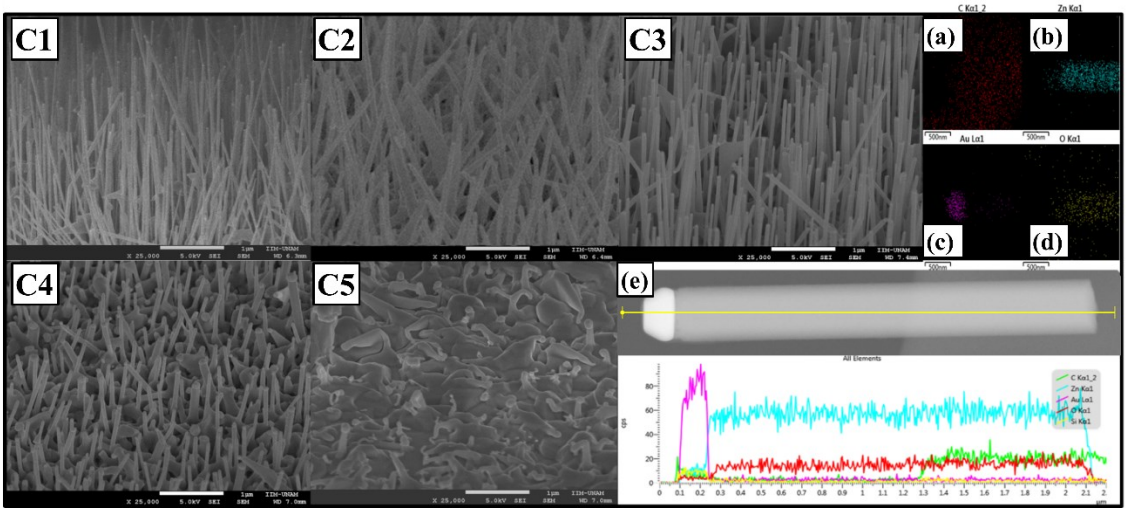

Fig. 2. C1-C5: SEM micrographs of ZnO NWs grown by sputtering technique (25,000 × magnification); EDX elementary mapping of C (a), Zn (b), Au (c), and C (d) of a single ZnO nanowire. (e) Compositional STEM profile of a single ZnO nanowire.

For sample C4, we can observe a lack of the anisotropic crystallization of ZnO. These samples allowed us to corroborate the fundamental role of the O_2/Ar mixture, which is used as a carrier gas during VLS growth [20]. The consequence of O_2 content on the development rate can be understood by considering the kinetics and thermodynamics associated with the catalyst drop of Au.

It is essential to mention that O_2 has no solubility in gold, neither in the solid-state nor in the liquid. Therefore, O_2 cannot reach the Au-ZnO (NWs) (growth interface) through diffusion via the catalyst drop. The elevated growth rate at a higher partial oxygen pressure is explained by a stable adhesion coefficient of the Zn atoms in the Au catalyst. Hereby, it can be expected that the growth mechanism is slightly different from the traditional VLS process. Proposed by Heike [32]: Zn forms an alloy only on the surface layers of the catalyst and diffuses by the curvature of the drop to the vapor-

catalyst-NW coexistence line. There, along with oxygen, the ZnO edges nucleate and grow laterally to the internal ZnO-Au interface regions, where both Zn and O diffuse and eventually promote the growth of NW in a kinetically controlled process.

The Au-ZnO interface is useful for ZnO NW development as the Zn (l) diffused through the Au catalyst drop can be finally used for the growth mechanism. An increment in the deposition rate infers a higher intake of Zn (l) by the Au catalyst, which, in turn, can decrease the amount of Zn (l) in the drop. Besides, a rise in the oxygen partial pressure causes a decrement in the fractional pressure of Zn on the Au-Zn catalyst. Consequently, the Zn vapor surpasses the steady pressure on the catalyst, escalating the amount of Zn atoms that adhere to Au. The quantity of Zn transported by the Au catalyst to the Au-ZnO heterointerface will upsurge until reaching stable deposition conditions; that is, the Zn supply and ZnO formation rates are equal. Therefore, the total of Zn in the metal catalyst is controlled by the amount of O_2 in the entrainment vapor, giving rise to a kinetically controlled mechanism.

Statistical analysis was performed on the SEM micrographs for the samples C1-C4 (Fig. 2). The outcomes are demonstrated in Table 1, where it can be seen the comparison of the aspect ratios of the four samples. In Fig. 2, we can see that in sample C5 small structures (Au nanoparticles) are formed at the tip of nanowires; however, their morphologies are not well-controlled, and their distribution is not homogeneous throughout the sample (small variation in the longitude and diameter observed in Table 1). In this sample, we can see the influence of the low substrate temperature. It is reported that one of the critical parameters to control the growth mechanism in VLS technique is the substrate temperature, which further determines the kinetics of epitaxial growth [36]. At temperatures below 650 °C, VLS growth cannot be achieved since there is not enough energy for the Au film to enter the liquid state and allow the diffusion of

Zn for the formation of nanostructures. The morphologies obtained at low temperatures must be obtained by a VS growth in which the precursor molecules are directly adsorbed on the solid surface of the substrate [37]. However, as previously mentioned by Kong et al., VS growths have the disadvantage of controlling the geometry, alignment, and precise location of ZnO nanostructures [38]. Since the morphologies of the obtained nanostructures in the sample C5 are quite distinct, statistical analysis was not made, and consequently, the aspect ratio for the same sample is not being reported here.

Fig. 2. (a-d) show STEM pictures of a ZnO nanowire obtained by the VLS technique (sample C1). This figure shows the EDX elementary mappings of elements such as C (a), Zn(b), Au(c), and O(d), respectively. Through these micrographs, we can determine that the tip of the nanowire contains Au, which corroborates the hypothesis that the path of growth of the nanowires was through the VLS technique. In order to understand how Zn spread within the drop of Au, as well as the possible diffusion of atoms of Au at the tip into the nanowire, an EDX scan was performed along the longitudinal axis of the nanowire. The image, together with the compositional profile, is shown in Fig. 2 (f). In this figure, we can see that there is a detectable amount of Zn inside the drop, and it signifies that the diffusion of this element to the growth interface occurred through the interior [39]. The carbon detected at the base of the structure corresponds to the TEM grid used during the measurement.

In the present VLS technique, it can also be seen that there is no considerable diffusion of Au throughout the structure, so we can consider the system as one where there is a metallization during the growth process. The deposition of noble metals on semiconductor structures is known as metallization. This process decreases the probability of electron-hole recombination, causes more proficient charge separation,

and thus, increases the response rate [8]. These metals can also assist in the process of electronic transfer, causing an increase in photocatalytic activity. As in comparison to the standard metallization process where the deposition of noble elements is carried out before the synthesis process, in the current case, VLS technique allowed us to obtain nanowires with in-situ metal nanoparticles on the tip. This result encourages the implementation of the systems obtained in photocatalysis applications such as hydrogen production or water treatment. In addition, the obtention of a well-defined ZnO/Au heterostructure in the present case suggests the presence of a plasmonic effect; however, specific further experiments are needed for a conclusive result.

Figure S2 presents a characteristic full binding energy spectrum (0-1100 eV) of the samples. In the spectra, peaks corresponding to the zinc orbitals: Zn3s, Zn3p, Zn3d, and Zn2p, the O1s oxygen orbital as well as the characteristic Auger lines of Zn: Zn LMM, Zn LMM1, Zn LMM2, and O KLL can be observed, corroborating presence of the forming elements of the semiconductor compound. Furthermore, the spectra also present the Au4f7 and C1s peaks, which verifies their presence on the surface of the nanowires. Furthermore, the deeper insight into the $Zn2p_{3/2}$ reveals the presence of Zn in multiple oxidation states, specifically the metallic form of Zn and the Zn^{2+} along with O^{2-} state.

3.3. Optical properties

Fig. 3 (a) displays the PL spectra of the different ZnO NWs. Higher intense emission between 450 - 660 nm can be observed. It is generally accepted that the source of the visible emission is the recombination of deep-level defects, so it is commonly referred to in the literature as deep-level emission (DLE). For example, the PL emission in the green area of the sample is frequently accredited to different known defects such as zinc vacancies (V_{Zn}) and oxygen vacancies (V_O) i.e., electrons recombine with

photopromoted holes to oxygen vacancies consequently producing the luminescence phenomenon [40]. On the other hand, blue-cyan emission, present in most of the samples is attributed in the literature to the transition between electrons in the CB with holes in oxygen anti-sites O_{Zn} [27, 34].

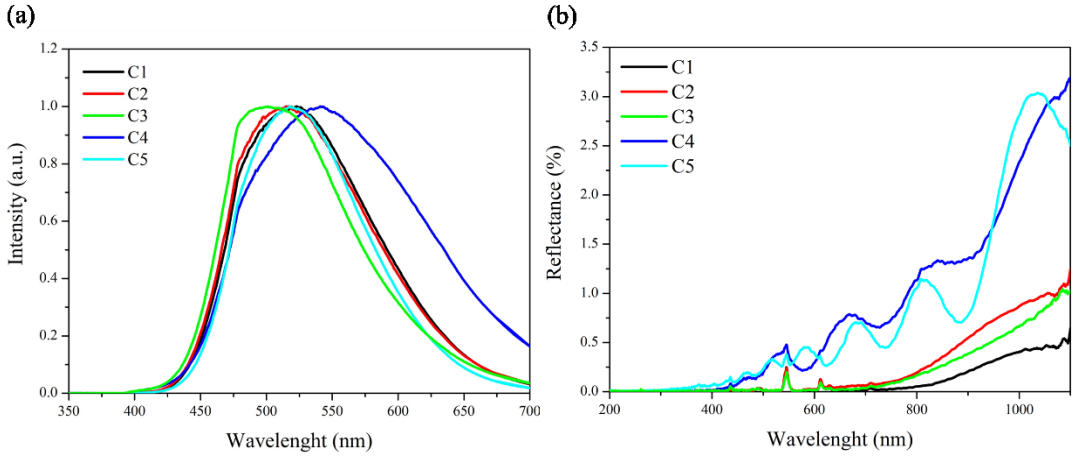

Fig. 3. (a) Room-temperature PL emission of ZnO nanowire arrays (C1 to C5). (b) UV-Visible (reflectance) spectra of the ZnO NWs.

Usually, PL emission depends on several factors such as surface morphology, crystal perfection, the stoichiometry of the material, doping, impurities, and different kinds of defect states, among others. A brief description of some of the defects is presented in Table 2.

Table 2. The relation between the different PL emission of the ZnO NWs and associated crystalline defects.

Energy (eV)	I(NBE)/I(DLE)	FWHM	Transition
Sample C1			
2.38	1.000	90	CB→V_O^+[40]
2.57	0.925	40	CB→O_{Zn}[41]
Sample C2			
2.16	1.000	120	CB→V_OZn_i[42]
2.55	0.845	26	CB→O_{Zn}[41]
Sample C3			
2.31	1.000	110	CB→ V_O^+[40]
Sample C4			

2.40	1.000	73	CB→ V_O^+[40]
2.17	1.106	97	CB→V_OZn_i[42]
2.58	0.929	40	CB→ O_{Zn} [41]
Sample C5			
2.57	1.000	82	CB→ O_{Zn} [41]
2.26	1.136	90	CB→ V_O^+[40]

Additionally, to the above-mentioned DLE emission band, ZnO also presents an excitonic band in the UV region of the spectra commonly referred to as NBE (near band edge excitonic). In order to estimate the contribution of the defect levels, the intensity ratio of the NBE and DLE bands was calculated [25]. Thus, for the ZnO nanowires presented in this work, the I (NBE)/I (DLE) ≈ 0.001, which means that DLE recombination significantly dominates.

In the earlier work [43], it was shown that the controlled defects within solid materials could be used as highly active photocatalytic sites for applications such as CO_2 reduction, N_2 fixation, and water splitting. This is commonly known as defect engineering. Specific molecular adsorption sites can be designed by the introduction of unsaturated defect sites in solid materials. Therefore, defect engineering is a promising method for the further advance of photocatalytic applications beyond hydrogen production.

The reflectance spectra of the ZnO nanowires are presented in Fig. 3 (b). Generally, in the case of ZnO semiconductor, absorption below 400 nm represents the intrinsic instigated by electron transition from the valence band to the conduction band. Samples with higher aspect ratios (C1, C2, C3) shown a decrement in the specular reflectance in the visible region, as is shown in Fig. 3 (b). In the spectra, it can also be seen that for samples C4 and C5, a more intense reflectance is displayed in comparison to the other three samples due to the more specular surface. Reflectance results infer that a better response due to the particular morphology of nanowires could also guarantee a better

light trapping and hence, improved photocatalytic response.

3.4. Photocatalytic proton reduction

We went on to study the ZnO thin films as photocatalysts for proton reduction from water in the existence of a hole scavenger. Using thin films rather than the typically used suspension systems has the advantage that it removes the need for agitation during the photocatalysis process, which will be valuable in future large-scale applications.

To understand the hydrogen evolution of the various ZnO NWs morphologies, we explore in detail their geometrical features calculating the volume and superficial area occupied by the NWs per μm^2 of geometric film area (based on their average length and diameter). The results are presented in Fig. 4. From these results, the active mass of the ZnO nanowires on the sample was estimated.

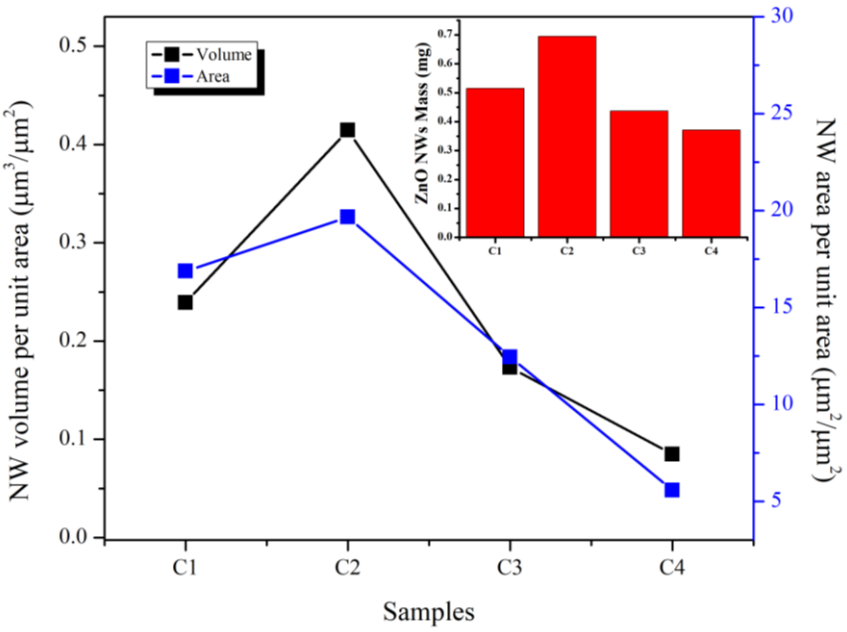

Fig. 4. (Left) Superficial area of the ZnO NWs per unit area of the substrate (Right) Volume per unit area ($1\mu m^2$) occupied by the ZnO NWs. (Inset) Estimated active mass (real) of the ZnO NWs.

All of the ZnO films produced hydrogen from water in the presence of a Na_2S/Na_2SO_3 mixture, acting as a hole-scavenger. Under these conditions C2 shows

the highest activity for hydrogen production (0.53 µmol cm^{-2}) under broadband illumination (λ > 295 nm, 300 W Xe light source), while all others show lower activities (C1: 0.37 µmol cm^{-2}, C3: 0.29 µmol cm^{-2}, C4: 0.37 µmol cm^{-2}, and C5: 0.22 µmol cm^{-2}; see Fig 5a) which shows good correlation with Fig. 4.

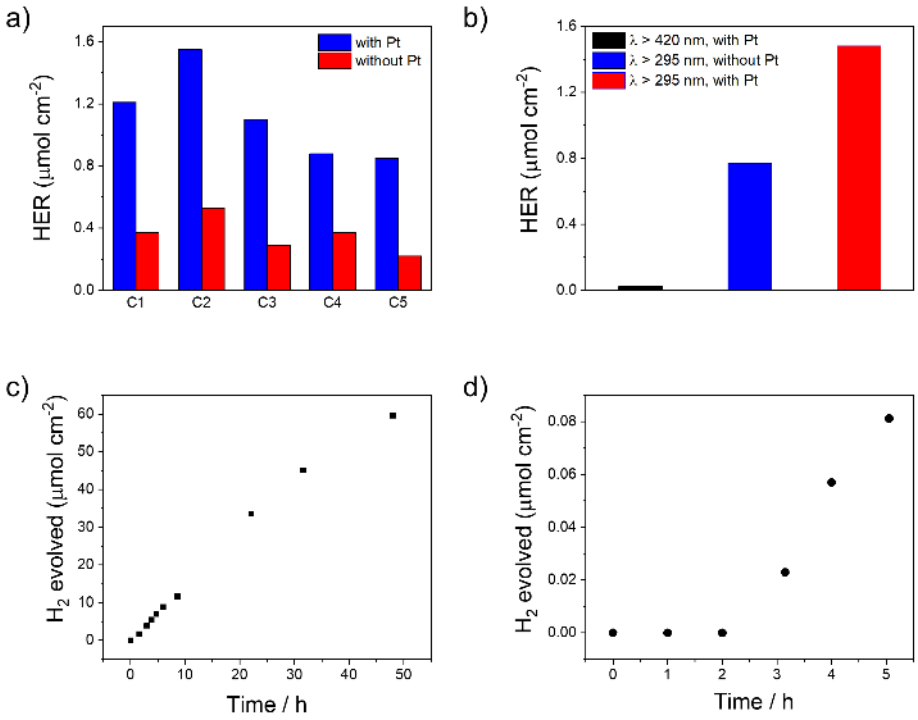

Fig. 5. a) Photocatalytic hydrogen evolution of the platinized ZnO films with additional platinum (from H_2PtCl_6 8 wt. % in H_2O,2 µL) from an 8 mL aqueous solution of Na_2S (0.35 M)/Na_2SO_3 (0.25 M) under broadband illumination (300 W, λ > 295 nm filter) for 5 hours illumination, red bar: without Pt, blue bar: with Pt; b) Photocatalytic hydrogen evolution of C2 under different conditions (λ > 420 nm, with Pt adding: black; λ > 295 nm, no Pt adding: blue; λ > 295 nm, with Pt adding: red); c) plot showing hydrogen evolution vs. time for C2 with Pt as co-catalyst under broadband illumination (λ > 295 nm); d) Photocatalytic hydrogen evolution of C2 with additional H_2PtCl_6 (from H_2PtCl_6 8 wt. % in H_2O, 2 µL) from an 8 mL aqueous solution of TEOA (10 vol%) under visible light illumination (300 W Xe light source, λ > 420 nm filter) for the first 2 hours, then under broadband illumination (λ > 295 nm filter) for further 5 hours.

No hydrogen production was observed under visible light for all films without additional co-catalyst. Upon addition of Pt via photo deposition from H_2PtCl_6 improved hydrogen evolution for all materials under broadband illumination was observed (C1: 1.21 μmol cm^{-2}, C2: 1.55 μmol cm^{-2}, C3: 1.10 μmol cm^{-2}, C4: 0.88 μmol cm^{-2} and C5: 0.85 μmol cm^{-2}; Fig. 5 a). The trend is comparable to the unplatanized samples, and activity was also found for the best performing material C2 with Pt co-catalyst under visible light (0.02 μmol cm^{-2}; Fig. 5 b).

It appears that the structuring of the ZnO films is beneficial, and the disordered sample (C5) has the lowest photocatalytic activity. For the ordered ZnO nanowires, an increase in performance is observed going from C1 to C2 before being lowered with reduced diameter.

It is, therefore, possible that differences in diameter (superficial area) affect the number of excitons generated, and being able to reach the interface, as well as light scattering within the films, play a role here.

We further went on to explore the stability of platinized C2 for 50 hours under broadband illumination (Fig. 5 c) and found that the photocatalytic activity does not change significantly throughout the run. When triethanolamine (TEOA) was used as the sacrificial hole scavengers, a decrease in performance was observed to 0.03 μmol cm^{-2} for platinized C2 (Fig. 5 d). A reduction in the activity of almost 52 times compared to experiments using Na_2S/Na_2SO_3 mixtures as the scavenger. No activity was observed under broadband illumination for C2 in the absence of a hole-scavenger. The stability of these photocatalysts was also studied by measuring UV-Vis, photoluminescence and FT-IR spectra before and after a photocatalytic hydrogen evolution experiment (Fig S-3 – Fig. S5). After 5 hours of photolysis a C2 sample

showed little change when comparing to the as made sample indicating good stability. In particular, we have found out that not only the high aspect ratio of the nanowires influence photocatalytic efficiency, but also the orientation to the substrate is a crucial factor. Trapping of light is enhanced in these random nanostructures, and it could subsequently enhance hydrogen evolution performance.

4. Conclusions

We examined the performance of various ZnO nanowire structures for photocatalytic hydrogen production from water splitting reaction. ZnO NWs with diameters ranging from 57 to 85 nm were synthesized by using VLS technique. The different morphologies of the arrays were obtained by varying the synthesis conditions during the deposition process and which further resulted in a change in the VLS growth regime to a VS dominant process (sample C5). Photocatalytic hydrogen evolution experiments were performed, and it was found that all materials act as catalysts in the existence of a sacrificial reagent under broadband illumination. Variations in the morphology, high aspect ratios, and preferential growth orientations, as well as an increase in absorbance and low reflectance in the visible region for the samples C1, C2, and C3, resulted in higher photocatalytic activity. Moreover, due to the large surface area and optimal diameter, sample C2 (random nanowires) showed stability and the uppermost performance in the hydrogen evolution from a water-splitting reaction.

Acknowledgments

A.G.M acknowledge CONACyT Scholarship CVU 860916. G.S. gratefully acknowledge the CONACyT project PN 4797. A.D. thank the DGAPA project PAPIIT IA100219. R.S.S thanks EPSRC for financial funding under Grant EP/N004884/1. Y.B. appreciates the CSC for a Ph.D. grant.

References

[1] Preethi V, Kanmani S. Photocatalytic hydrogen production. Mater Sci Semicond Process 2013;16:561–75. https://doi.org/10.1016/j.mssp.2013.02.001.

[2] Liao C-H, Huang C-W, Wu JCS. Hydrogen Production from Semiconductor-based Photocatalysis via Water Splitting. Catalysts 2012;2:490–516. https://doi.org/10.3390/catal2040490.

[3] Tentu RD, Basu S. Photocatalytic water splitting for hydrogen production. Curr Opin Electrochem 2017;5:56–62. https://doi.org/10.1016/j.coelec.2017.10.019.

[4] Haryanto A, Fernando S, Murali N, Adhikari S. Current status of hydrogen production techniques by steam reforming of ethanol: A review. Energy and Fuels 2005;19:2098–106. https://doi.org/10.1021/ef0500538.

[5] Fujishima A, Honda K. Electrochemical Photolysis of Water at a Semiconductor Electrode. Nature 1972;240:226–9. https://doi.org/10.1038/239137a0.

[6] Zhang K, Guo L. Metal sulphide semiconductors for photocatalytic hydrogen production. Catal Sci Technol 2013;3:1672–90. https://doi.org/10.1039/c3cy00018d.

[7] Chiarello GL, Dozzi M V., Selli E. TiO2-based materials for photocatalytic hydrogen production. J Energy Chem 2017;26:250–8. https://doi.org/10.1016/j.jechem.2017.02.005.

[8] Ameta R, Ameta S. Photocatalysis: principles and applications. CRC Press; 2017.

[9] Ni M, Leung MKH, Leung DYC, Sumathy K. A review and recent developments in photocatalytic water-splitting using TiO2for hydrogen production. Renew Sustain Energy Rev 2007;11:401–25. https://doi.org/10.1016/j.rser.2005.01.009.

[10] Chen WF, Muckerman JT, Fujita E. Recent developments in transition metal carbides and nitrides as hydrogen evolution electrocatalysts. Chem Commun 2013;49:8896–909. https://doi.org/10.1039/c3cc44076a.

[11] Merki D, Fierro S, Vrubel H, Hu X. Amorphous molybdenum sulfide films as catalysts for electrochemical hydrogen production in water. Chem Sci 2011;2:1262–7. https://doi.org/10.1039/c1sc00117e.

[12] Akhundi A, Badiei A, Ziarani GM, Habibi-Yangjeh A, Muñoz-Batista MJ, Luque R. Graphitic carbon nitride-based photocatalysts: Toward efficient organic transformation for value-added chemicals production. Mol Catal 2020;488:110902. https://doi.org/10.1016/j.mcat.2020.110902.

[13] Maeda K, Higashi M, Lu D, Abe R, Soc AJAC. Photoexcitation by Visible Light using a Modified Oxynitride as a Hydrogen Evolution Photocatalyst. J Am Chem Soc 2010;132:5858–68.

[14] Samadi M, Zirak M, Naseri A, Khorashadizade E, Moshfegh AZ. Recent progress on doped ZnO nanostructures for visible-light photocatalysis. Thin Solid Films 2016;605:2–19. https://doi.org/10.1016/j.tsf.2015.12.064.

[15] Wang ZL. Novel Nanostructures and Nanodevices of ZnO. Zinc Oxide Bulk, Thin Film. Nanostructures, Elsevier; 2006, p. 339–70. https://doi.org/10.1016/B978-008044722-3/50010-5.

[16] Hou TF, Johar MA, Boppella R, Hassan MA, Patil SJ, Ryu SW, et al. Vertically aligned one-dimensional ZnO/V2O5 core–shell hetero-nanostructure for

photoelectrochemical water splitting. J Energy Chem 2020;49:262–74. https://doi.org/10.1016/j.jechem.2020.02.004.

[17] Jayah NA, Yahaya H, Mahmood MR, Terasako T, Yasui K, Hashim AM. High electron mobility and low carrier concentration of hydrothermally grown ZnO thin films on seeded a-plane sapphire at low temperature. Nanoscale Res Lett 2015;10:1–10. https://doi.org/10.1186/s11671-014-0715-0.

[18] Rokade A, Rondiya S, Sharma V, Prasad M, Pathan H, Jadkar S. Electrochemical synthesis of 1D ZnO nanoarchitectures and their role in efficient photoelectrochemical splitting of water. J Solid State Electrochem 2017;21:2639–48. https://doi.org/10.1007/s10008-016-3427-9.

[19] Shekofteh-Gohari M, Habibi-Yangjeh A, Abitorabi M, Rouhi A. Magnetically separable nanocomposites based on ZnO and their applications in photocatalytic processes: A review. Crit Rev Environ Sci Technol 2018;48:806–57. https://doi.org/10.1080/10643389.2018.1487227.

[20] Teh SJ, Lai CW, Hamid SBA. Novel layer-by-layer assembly of rGO-hybridised ZnO sandwich thin films for the improvement of photo-catalysed hydrogen production. J Energy Chem 2016;25:336–44. https://doi.org/10.1016/j.jechem.2016.01.009.

[21] Yang PYP. Semiconductor nanowires for energy conversion. Nanoelectron Conf (INEC), 2010 3rd Int 2010:527–46. https://doi.org/10.1109/INEC.2010.5424441.

[22] Govatsi K, Seferlis A, Neophytides SG, Yannopoulos SN. Influence of the morphology of ZnO nanowires on the photoelectrochemical water splitting efficiency. Int J Hydrogen Energy 2018;43:4866–79. https://doi.org/10.1016/j.ijhydene.2018.01.087.

[23] Guo S, Li X, Zhu J, Tong T, Wei B. Au NPs@MoS2 Sub-Micrometer Sphere-ZnO Nanorod Hybrid Structures for Efficient Photocatalytic Hydrogen Evolution with Excellent Stability. Small 2016;12:5692–701. https://doi.org/10.1002/smll.201602122.

[24] Awazu K, Fujimaki M, Rockstuhl C, Tominaga J, Murakami H, Ohki Y, et al. A plasmonic photocatalyst consisting of silver nanoparticles embedded in titanium dioxide. J Am Chem Soc 2008;130:1676–80. https://doi.org/10.1021/ja076503n.

[25] Pirhashemi M, Habibi-Yangjeh A, Rahim Pouran S. Review on the criteria anticipated for the fabrication of highly efficient ZnO-based visible-light-driven photocatalysts. J Ind Eng Chem 2018;62:1–25. https://doi.org/10.1016/j.jiec.2018.01.012.

[26] Liu E, Kang L, Yang Y, Sun T, Hu X, Zhu C, et al. Plasmonic Ag deposited TiO 2 nano-sheet film for enhanced photocatalytic hydrogen production by water splitting. Nanotechnology 2014;25. https://doi.org/10.1088/0957-4484/25/16/165401.

[27] Shi Y, Wang J, Wang C, Zhai TT, Bao WJ, Xu JJ, et al. Hot Electron of Au Nanorods Activates the Electrocatalysis of Hydrogen Evolution on MoS<inf>2</inf> Nanosheets. J Am Chem Soc 2015;137:7365–70. https://doi.org/10.1021/jacs.5b01732.

[28] Serrano A, Arana A, Galdámez A, Dutt A, Monroy BM, Güell F, et al. Effect of

the seed layer on the growth and orientation of the ZnO nanowires: Consequence on structural and optical properties. Vacuum 2017;146:509–16. https://doi.org/10.1016/j.vacuum.2017.03.010.

[29] Zhang X, Li Y, Zhao J, Wang S, Li Y, Dai H, et al. Advanced three-component ZnO/Ag/CdS nanocomposite photoanode for photocatalytic water splitting. J Power Sources 2014;269:466–72. https://doi.org/10.1016/j.jpowsour.2014.06.165.

[30] Muñoz-Fernandez L, Sierra-Fernandez A, Milošević O, Rabanal ME. Solvothermal synthesis of Ag/ZnO and Pt/ZnO nanocomposites and comparison of their photocatalytic behaviors on dyes degradation. Adv Powder Technol 2016;27:983–93. https://doi.org/10.1016/j.apt.2016.03.021.

[31] Zhang N, Shan CX, Tan HQ, Zhao Q, Wang SP, Sun ZC, et al. Black-colored ZnO nanowires with enhanced photocatalytic hydrogen evolution. Nanotechnology 2016;27:1–6. https://doi.org/10.1088/0957-4484/27/22/22LT01.

[32] Simon H, Krekeler T, Schaan G, Mader W. Metal-seeded growth mechanism of ZnO nanowires. Cryst Growth Des 2013;13:572–80. https://doi.org/10.1021/cg301640v.

[33] Galdámez-Martinez A, Santana G, Güell F, Martínez-Alanis PR, Dutt A. Photoluminescence of zno nanowires: A review. Nanomaterials 2020;10:857. https://doi.org/10.3390/nano10050857.

[34] Sprick RS, Cheetham KJ, Bai Y, Alves Fernandes J, Barnes M, Bradley JW, et al. Polymer photocatalysts with plasma-enhanced activity. J Mater Chem A 2020;8:7125–9. https://doi.org/10.1039/d0ta01200a.

[35] Patterson AL. The scherrer formula for X-ray particle size determination. Phys Rev 1939;56:978–82. https://doi.org/10.1103/PhysRev.56.978.

[36] Menzel A, Subannajui K, Bakhda R, Wang Y, Thomann R, Zacharias M. Tuning the growth mechanism of ZnO nanowires by controlled carrier and reaction gas modulation in thermal CVD. J Phys Chem Lett 2012;3:2815–21. https://doi.org/10.1021/jz301103s.

[37] Khan MA, Sakrani S. Jurnal Teknologi Full paper Synthesis of Cu 2 O and ZnO Nanowires and their Heterojunction Nanowires by Thermal Evaporation : A Short Review 2014;5:83–8. https://doi.org/10.11113/jt.v71.3861.

[38] Kong XY, Wang ZL. Spontaneous Polarization-Induced Nanohelixes, Nanosprings, and Nanorings of Piezoelectric Nanobelts. Nano Lett 2003;3:1625–31. https://doi.org/10.1021/nl034463p.

[39] Barth S, Hernandez-ramirez F, Holmes JD, Romano-rodriguez A. Progress in Materials Science Synthesis and applications of one-dimensional semiconductors. Prog Mater Sci 2010;55:563–627. https://doi.org/10.1016/j.pmatsci.2010.02.001.

[40] Ahn CH, Kim YY, Kim DC, Mohanta SK, Cho HK. Erratum: A comparative analysis of deep level emission in ZnO layers deposited by various methods (Journal of Applied Physics (2009) 105 (013502)). J Appl Phys 2009;105. https://doi.org/10.1063/1.3112042.

[41] Wang DF, Zhang TJ. Study on the defects of ZnO nanowire. Solid State Commun 2009;149:1947–9. https://doi.org/10.1016/j.ssc.2009.07.038.
[42] Djurišić AB, Leung YH. Optical properties of ZnO nanostructures. Small 2006;2:944–61. https://doi.org/10.1002/smll.200600134.
[43] Zhang N, Gao C, Xiong Y. Defect engineering: A versatile tool for tuning the activation of key molecules in photocatalytic reactions. J Energy Chem 2019;37:43–57. https://doi.org/10.1016/j.jechem.2018.09.010.